Journal of Alloys and Compounds 511 (2012) 169–175

Contents lists available at SciVerse ScienceDirect

Journal of Alloys and Compounds

journal homepage: www.elsevier.com/locate/jallcom

Structure and hydrogen absorbing properties of ScCrMn alloy

Wuhui Li, Erdong Wu*

Shenyang National Laboratory for Material Science, Institute of Metal Research, Chinese Academy of Sciences, 72 Wenhua Road, Shenhe District, Shenyang 110016, China

ARTICLE INFO

Article history:
Received 18 July 2011
Received in revised form 8 September 2011
Accepted 8 September 2011
Available online 16 September 2011

Keywords:
Sc-based Laves phase alloy
Crystal structure
Hydrogen activation
Hydrogen absorption/desorption
Thermodynamics

ABSTRACT

The crystal structures of ScCrMn alloy and its hydride are determined by XRD Rietveld analysis and TEM examination. The ScCrMn alloy exhibits a rarely ideal close-packed C14 type hexagonal Laves phase structure with lattice parameters $a = 5.064(1)$, $c = 8.263(2)$ Å, deviating from the ANOE dependent rule on Laves phase structure. The hydrogenation of the alloy to $ScCrMnH_{3.9}$ results in significant lattice expansion of 27%, but does not alter the matrix lattice structure. The XRD pattern of the hydride also shows close-packed structure with little line broadening, comparable to that of the alloy, indicating a high degree of crystallinity, where the hydrogen atoms are homogeneously distributed in evenly distributed interstitials with minimal defects. The alloy demonstrates extremely easy activation property. The alloy can be activated at a low pressure of 0.46 kPa and exhibit very fast absorption rate at sub-atmosphere at room temperature. The hydrogenation thermodynamics of the alloy are evaluated by *P–C–T* measurements at different temperatures. At hydrogen concentration H/M = 0.66 corresponding to a defined room temperature plateau pressure, the relative partial molar enthalpy ΔH and entropy ΔS derived by Van't Hoff equation are −63 kJ/mol and −111 J/mol K, respectively. These results manifest that the hydride stability of the ScCrMn alloy is comparable to those of the hydrogen isotope storage alloys of ZrCo and $ZrTi_{0.2}V_{1.8}$, and would be superior on relevant applications. The DSC–TG measurements of the hydride reveal that the total release of hydrogen can basically be achieved at 653 K, accompanied by an oxidation reaction with residual oxygen to form water vapor. The results indicate that the alloy is an effective catalyst for the dissociation of hydrogen and combination of oxygen.

1. Introduction

The Ti- and Zr-based Laves phase alloys have been extensively studied on hydrogen storage properties due to their fast kinetics, high storage capacity, easy activation, moderate working conditions and existence of wide ranges of homogeneity [1–4]. Among these alloys, the $Ti_xZr_{1-x}MnCr$ alloys have been studied recently [5,6]. It is found that the $Ti_xZr_{1-x}MnCr$ alloys have relatively high reversible hydrogen storage capacities, good thermodynamics and plateau characteristics. In particular, the $Ti_{0.68}Zr_{0.32}MnCr$ alloy exhibits favorable balanced hydrogenation properties [5,6]. However, the Ti-based alloys usually encounter difficulties in activation due to the formation of dense oxides and hydroxides on the alloy surfaces during air exposure, and have to substitute Zr or some rare earth metals to overcome the problems [7,8]. The Zr and most rare earth metals are relatively heavy, and would reduce the hydrogen storage capacity of the alloys. Therefore, in order to improve the hydrogen activation and seek novel hydrogen storage properties, we turn our attention to the Sc-based Laves phase alloys.

The previous studies of Sc in Laves phase hydrogen storage alloys have covered the $ScMn_2$ [9], the ScM_2 (M = Fe, Co and Ni) [10], the ScZr-based alloy [11], the ScB_2 ($B_2 = Ni_{1.1}Co_{0.2}Mn_{0.5}Cr_{0.2}$) [12] and the $Ti(Zr)_xSc_{1-x}Fe_2$ ($x = 0.8$ and 0.5) [13]. On the other hand, as the Lave phase ZrMnCr alloy exhibits good activation properties, whereas the corresponding ScCrMn alloy has not been reported so far to our knowledge, we start with the ScCrMn alloy. According to the Sc based binary phase diagrams, there is no Laves phase in Sc–Cr system. However, Sc and Mn can form a C14 type Laves phase $ScMn_2$ and two other intermetallic compounds Sc_6Mn_{23} and Sc_4Mn.

In the studies described in this paper, the crystal structures of the ScCrMn alloy and its hydride are determined by X-ray diffraction and electron microscopic measurements. The activation property of the alloy is estimated by time dependent hydrogen absorption measurements, the hydrogen absorption properties and the enthalpies of formation of the hydrides are determined by *P–C–T* measurements, and the hydrogen releasing process of the hydride is revealed by the DSC and TG measurements.

2. Experimental

30 g sample of ScCrMn alloy was prepared by arc melting the component element ingots under a Ti-gettered Ar atmosphere in a water-cooled copper crucible.

* Corresponding author. Tel.: +86 24 23971952; fax: +86 24 23971215.
E-mail address: ewu@imr.ac.cn (E. Wu).

0925-8388/$ – see front matter © 2011 Elsevier B.V. All rights reserved.
doi:10.1016/j.jallcom.2011.09.023

The sample was overturned and remelted three times to ensure homogeneity. The purities of the ingots were Sc 99.90%, Mn 99.90% and Cr 99.98%, respectively. An excess amount of Mn controlled to 9% was added to compensate the weight loss during melting. The crystal structures of the alloy and its hydride were characterized by XRD using Cu K_α radiation in a Rigaku diffractometer, and the data were analyzed using a Rietveld program LHPM [14]. The microstructures and compositions were confirmed by SEM (Quanta 600) and TEM (Tecnai F20).

The hydrogen absorption and desorption measurements were carried out in a Sievert's apparatus. About 0.6 g bulk sample was used for activation and about 1.2 g bulk sample for *P–C–T* measurements. The activation was performed at 298 ± 1 K, whereas the hydrogen capacity and *P–C–T* characteristics were measured at 571 K, 400 K, 433 K, 471 K, 508 K, and 298 K under pressure range of 0.01–110 kPa. The system was evacuated by rotary pump for 30 min prior to activation, and six hydrogen charge–discharge cycles were operated for the *P–C–T* measurement after the initial activation. After each cycle, the sample was degassed at 653 K under a vacuum of several Pa based on the thermal gravity analyses. The plateau pressure was defined as the pressure at the half of the hydrogen absorption capacity at 100 kPa.

The DSC and TG measurements (NETSCH STA 449F3) of the hydride were carried out in atmospheric Ar. During measurements, the system was purged by high purity Ar (99.999%) for 0.5 h, and then heated at a rate of 10 K/min and kept at 653 K for 40 min. The released gases during the DSC–TG measurements were measured in situ by an attached mass spectrometer. The hydrogen concentration in the hydride was also determined by a RH-404 hydrogen determinator (LECO). The determination was based on inert gas fusion method, in which the hydrogen was quantified by impulse furnace heating - thermal conductivity. The determinator had an accuracy of ±0.05 ppm (or 2% of the reading, whichever was higher) [15].

3. Results and discussion

3.1. The crystal structures of ScCrMn alloy and its hydrides

3.1.1. XRD analysis

The Rietveld fits of the XRD patterns of the ScCrMn alloy and its hydride $ScCrMnH_{3.9}$ are shown in Fig. 1, and the derived crystal structural parameters are listed in Table 1. The crystal structures of ScCrMn and $ScCrMnH_{3.9}$ are determined to be C14-type Laves phase (space group $P6_3/mmc$) with 4 formulas in each unit cell. A trace amount (~1 wt%) of Sc_2O_3 can be identified from the XRD patterns of both the alloy and its hydride.

The Laves phases crystallize in three structure types, which are named after the representatives cubic $MgCu_2$ (C15), hexagonal $MgZn_2$ (C14) and hexagonal $MgNi_2$ (C36). It is suggested that the structure of the phase is dependent on the averaged number of outer electrons (ANOE) [16]. According to the generalized rules based on the Zr-based and Ti-based alloys, the ScCrMn with ANOE = 5.3 would more likely to form a cubic C15 structure. However, ScCrMn follows the ZrMnCr and $ScMn_2$ alloys possessing a C14 structure, and there is no sign of structural modification indicating ordering of the Cr and Mn atoms in the structure. Therefore, ScCrMn can be regarded to be formed by replacing Zr in ZrMnCr with Sc or by randomly substituting half Mn with Cr in $ScMn_2$, corresponding to an exact formula of $Sc(Cr_{0.5}Mn_{0.5})_2$. The lower electron valence of the Sc or Cr atoms in the substitution does not alter the original C14 structure, implying that other factor rather than ANOE dominates in the formation of C14 structure in this case.

It is known that an ideal close-packed C14 type AB_2 Laves phase structure would have a unit cell axis c/a ratio of 1.633, and a ratio of the atomic radius of A to B atoms of 1.225. It is interesting to note that the unit cell of ScCrMn alloy has a c/a ratio of 1.632. The reported atomic radii of Sc, Cr and Mn are 1.62, 1.30 and 1.35 Å, respectively [17]. In the derived unit cell of ScCrMn, the Sc atoms are at the ideal positions, whereas the x coordinates of Mn and Cr atoms only deviate about 0.5% from the ideal values of 5/6, etc. The atomic radii of Sc and Cr/Mn are estimated to be 1.554 and 1.298 Å, respectively, leading to an atomic radius ratio of Sc to Cr and Mn of 1.197. These structural parameters meet the ideal values almost perfectly, hence provide a rare example of ideal close-packed C14 type hexagonal Laves phase structure. Consequently, the properties, in particular the hydrogenation properties, of the alloy, will be affected by the ideal close-packed structure.

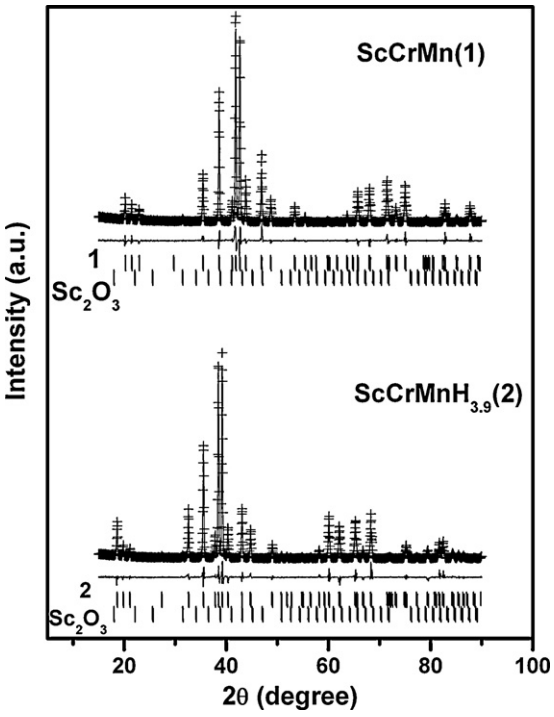

Fig. 1. The refinement of the XRD pattern for ScCrMn and $ScCrMnH_{3.9}$. Data points are shown as + and the calculated as a solid line. The difference profile for the refinement, along with reflection markers for the identified phases, is shown below each pattern.

The particle size and lattice strain of a sample are associated with the line broadening measured by the values of full width at half maximum (FWHM) of XRD reflections. In comparison with the FWHM values of 0.160°(37.70° (2θ)) and 0.157°(43.28°) for the (1 1 0) and (1 1 3) reflections of a standard Al_2O_3 sample, the FWHM values of the (0 1 3) and (0 2 1) reflections at similar 2θ for ScCrMn are 0.171°(38.56°) and 0.172°(42.63°), respectively. Since the line broadening in the reflections of standard Al_2O_3 is negligent, the comparable FWHM values for ScCrMn indicate that the alloy has little lattice strain. In the XRD patterns of the $Ti_xZr_{1-x}MnCr$ alloys, the dependence of lattice strain on the Ti content x, and the

Table 1
Crystal structure parameters of ScCrMn and $ScCrMnH_{3.9}$ derived by Rietveld refinements. The standard deviations of the structural parameters are in the parentheses. The symbols of q and B_{iso} correspond to the site occupancy and isotropic temperature factor, respectively.

Structural information	ScCrMn	$ScCrMnH_{3.9}$
Space group: $P6_3/mmc$ (194)	a = 5.064(1) Å, c = 8.263(2) Å, c/a = 1.632(2), V = 183.5(2) Å^3	a = 5.493(1) Å, c = 8.949(2) Å, c/a = 1.629(2), V = 233.8(2) Å^3
Sc: x, y, z, q, B_{iso}	4(f): 1/3, 2/3, 0.438(1), 1, 1.5	4(f): 1/3, 2/3, 0.436(2), 1, 1.7
Cr/Mn: x, y, z, q, B_{iso}	2(a): 0, 0, 0, 1, 1.3	2(a): 0, 0, 0, 1, 2.0
Cr/Mn: x, y, z, q, B_{iso}	6(h): 0.829(1), 2x, 1/4, 1, 1.4	6(h): 0.836(1), 2x, 1/4, 1, 1.7
R_{wp} (%)	16.2	15.1
R_B (%)	6.2	5.5
Impurities (wt%)	Sc_2O_3 1.1	Sc_2O_3 1.0

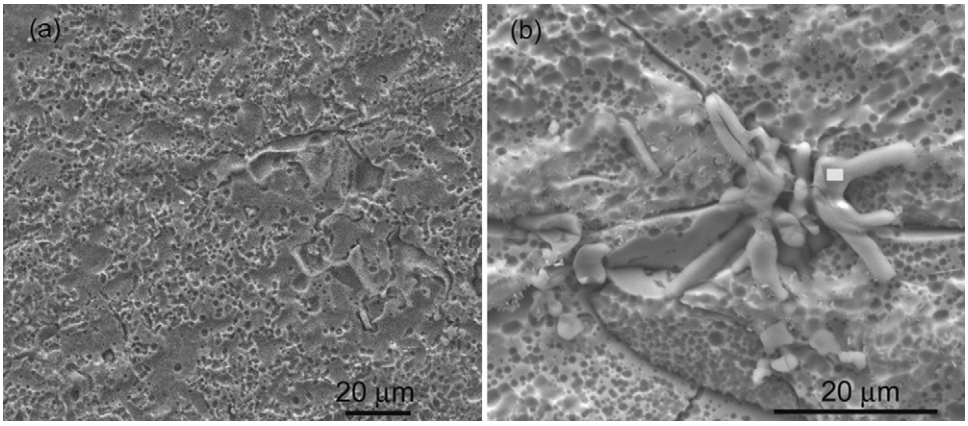

Fig. 2. The SEM images of ScCrMn alloy surface, (a) an image taken at 2000×, and the EDS is scanned for the whole area; (b) another image taken at 5000×, and the EDS is focused at a local area marked by the white square.

appearance of maximum lattice strain at $x = 0.5$ have been observed, and attributed to the large difference between the sizes of the Ti and Zr atoms [5]. Therefore, the nearly identical sizes of the Mn and Cr atoms would be the main cause of the low lattice strain in the alloy. In addition, the ideal close-packed structure would also be a contributing factor.

For the hydride of $ScCrMnH_{3.9}$, the determined C14-type structure indicates that the hydrogenation of the alloy does not alter the matrix lattice structure. The derived structural parameters of the hydride are very similar to that of the alloy, with nearly ideal values for the close-packed C14 structure. Although the metal atoms in the hydride are not close-packed any more due to the expanded unit-cell, such structure feature suggests that the hydrogen atoms are homogeneously distributed in evenly distributed interstitials of the hydride. On the other hand, although the volume of the hydride increases by 27% compared to that of the alloy, the XRD pattern of the hydride does not show observable broadening. However, careful analysis reveals that although the average FWHM value of the hydride is unchanged and even smaller, there are slight variations for the individual reflections. For example, the FWHM values of (0 1 3) and (0 2 1) reflections of $ScMnCrH_{3.9}$ become 0.183°(35.50°) and 0.148°(39.16°), respectively, indicating different indices dependence and minor broadening anisotropy. Extra lattice strain is usually induced in the hydrogen absorption of the transition and rare earth metal alloys due to inhomogeneous distribution of hydrogen in interstitial sites and formation of various types of defects. For example, strong anisotropic broadening is observed in the hydride of typical hydrogen storage alloy $LaNi_5$ [18], whereas the line broadening have been observed in the hydrides of several Laves phase alloys [19,20]. However, in the study of a similar hydride of $ScFe_2$, though both the alloy and its hydride have shown considerable line broadening, the differences between them are undetected. The low and comparable FWHM values of the reflections of the hydride of ScCrMn alloy indicate that the hydride possesses a high degree of crystallinity with minimal serious lattice defects.

3.1.2. SEM and TEM examinations

The polished surfaces of the ScCrMn alloy mildly etched by mixed strong acid are displayed in Fig. 2, and the corresponding EDS results are presented in Table 2. The EDS data manifest that the detected compositions of the ScCrMn sample are very close to that of the fabrication design, with acceptable deviations of within 0.5%. The surface of the alloy after etching is rough, containing many pits and some isolated inclusions. In a local area of the surface, the inclusions are identified to be Sc_2O_3, consistent with the analysis of XRD.

Fig. 3 shows a series of SAED patterns of the ScCrMn alloys obtained from the TEM examination. The crystal structure and lattice parameters derived from XRD can be cross-checked with the analysis of these patterns. The discernible 6 fold symmetry in (*a*) conforms that the hexagonal structure of the crystal. The extinction of the (0 0 1) plane in (*b*) indicates the existence of screw axis, consistent with the feature of the space group of $P6_3/mmc$. The appearance of unexpected faint alternate spots associated to the (0 0 1) planes in (*c*) can be attributed to the dynamical scattering events due to the thick specimen. The lattice parameters of $a = 5.07$ Å and $c = 8.27$ Å obtained from the indexing of the patterns agree well with the XRD derived values of $a = 5.064$ Å and $c = 8.263$ Å.

Fig. 4 presents a typical platelet-like single crystal particle of the ScCrMn hydride and the corresponding $[1\bar{2}0]$ SAED pattern. The large dimension of about 1.6 μm for the particle and the relatively distinct diffraction spots confirm that the hydride of the alloy has retained large particle size and a high degree of crystallinity after hydrogenation. The SAED pattern is similar to that of the alloy, and the indexing is consistent with the XRD result.

3.2. Hydrogen absorption properties of ScCrMn

3.2.1. Activation properties

Fig. 5(a) shows the kinetics for the initial hydrogen uptake at a subatmospheric pressure of 98.6 kPa without prior treatment of the alloy. The half-time for the full initial absorption is 16.5 s including an incubation time of 6 s. The reaction rate speeds up after the incubation, reaches a maximum at about 16 s, and become slower afterwards. Fig. 5(b) presents repeated charges of hydrogen at a low pressure of about 0.46 kPa, which provide a measure for the easiness of the activation. It shows that even at such a low pressure, the first hydrogenation curve still has the same absorption character of that at higher pressure. The existence of an incubation time and a maximum rate in the initial absorption indicates that the activation process is self-accelerating. The activation is likely to proceed through a hydrogen adsorption induced cracking mechanism to overcome the thick oxide layer on the surface of the bulk sample. On the other hand, the extremely high reaction

Table 2
Compositions of element from EDS of SEM.

	Alloy			
	Sc (at.%)	Cr (at.%)	Mn (at.%)	O (at.%)
Whole photo area	33.0	33.3	33.7	8.2 (excluded)
Local area	40.4	0.7	0.7	58.2

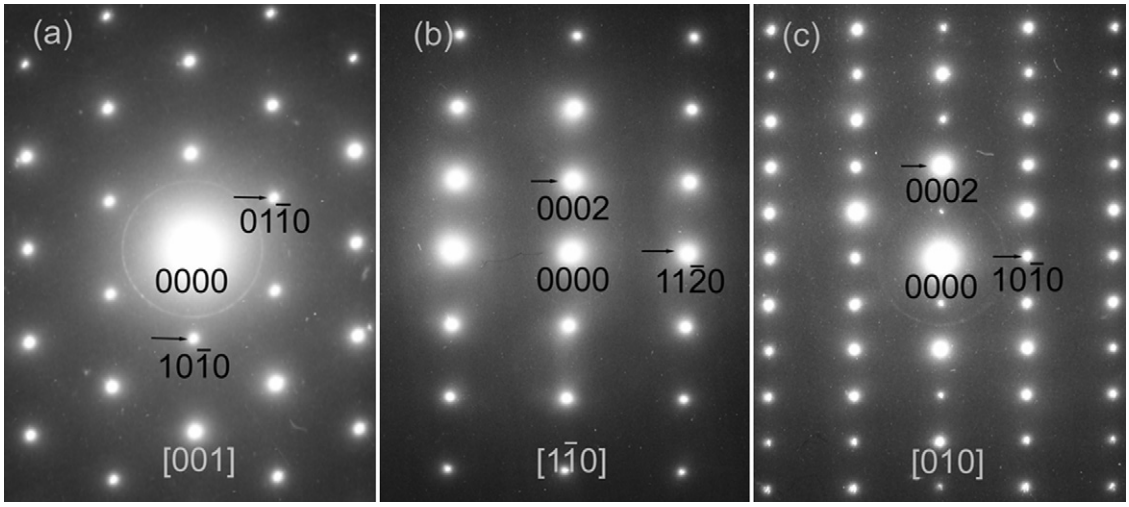

Fig. 3. SAED patterns of ScCrMn alloy, where the corresponding zone axis is displayed on the bottom of each patterns.

rate of the hydrogenation exhibited at low pressure and room temperature suggest that the ScCrMn alloy is a very strong catalyst for the dissociation of hydrogen molecules.

3.2.2. Hydrogen absorption/desorption behavior

The hydrogen absorption/desorption isotherms of the ScCrMn alloy are presented in Fig. 6. The hydrogen absorption capacity at 298 K and 100 kPa is 1.33 H/M, corresponding to a hydride of $ScCrMnH_4$. This value decreases with increasing temperature, and to 0.68 H/M at 571 K. On the other hand, the absorption/desorption hysteresis also decreases with temperature. This character of hysteresis is as same as that of the Pd–H_2 system [21], but opposite to the $LaNi_5$–H_2 system [22], where the hysteresis increases with increasing temperature. It has been suggested that the desorption curves represent the true strain-free equilibrium, whereas the absorption curves represent, instead, an equilibrium under mechanical constraints [21]. In the absorption/desorption isotherms of ScCrMn-H_2, the obvious hysteresis observed in the limited data of the desorption curve at 298 K indicates that there exists considerable strain under desorption equilibrium at room temperature. However, the hysteresis is reduced significantly at 400 K, and basically disappeared at 478 K, instructing the hysteresis critical temperature at this temperature. In comparison, the hysteresis critical temperature for the Pd–D_2 system is about 543 K [21]. The relatively quick reduction of hysteresis and low critical temperature indicate that the temperature effect on the mechanical strain in the hydrogen desorption equilibrium is strong. On the other hand, the presence of $\alpha + \beta$ and β phase regions at various temperatures can be perceived from the absorption isotherms, though the isotherms exhibit rather slope plateaus. The observed plateau pressures of the alloy are quite low, varying from about 0.01 kPa at 298 K to 17 kPa at 571 K. According to a general rule, the larger the lattice parameter of the alloy, the lower plateau pressure and higher stability the hydriding system has [23]. The lattice parameters of ScCrMn are close to those of ZrMnCr [24], implying similar atomic sizes between the Sc and Zr atoms in the crystal

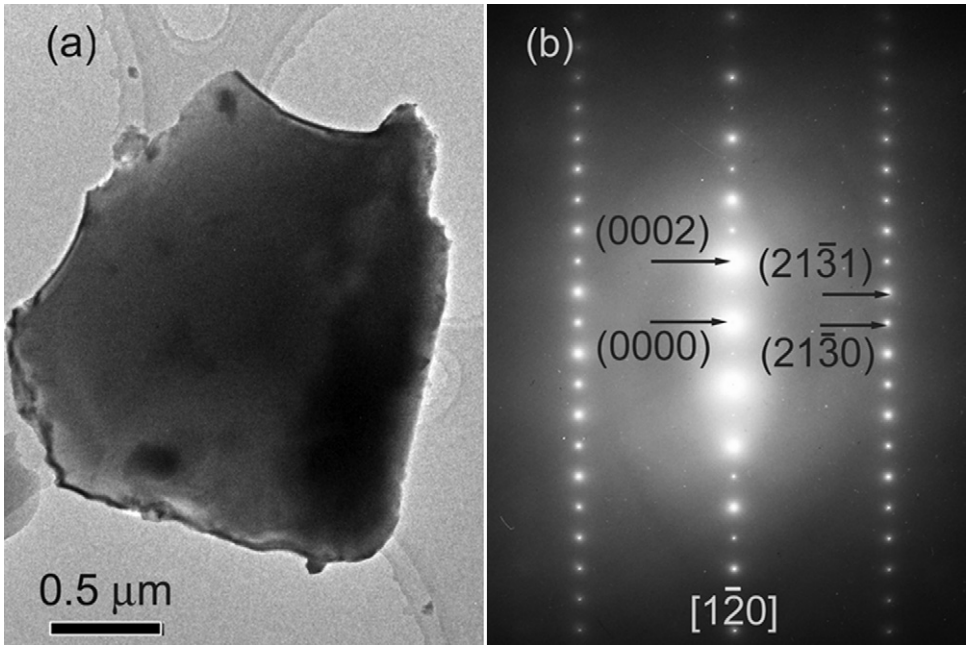

Fig. 4. (a) Bright field image, and (b) corresponding SAED pattern of a particle of ScCrMn hydride.

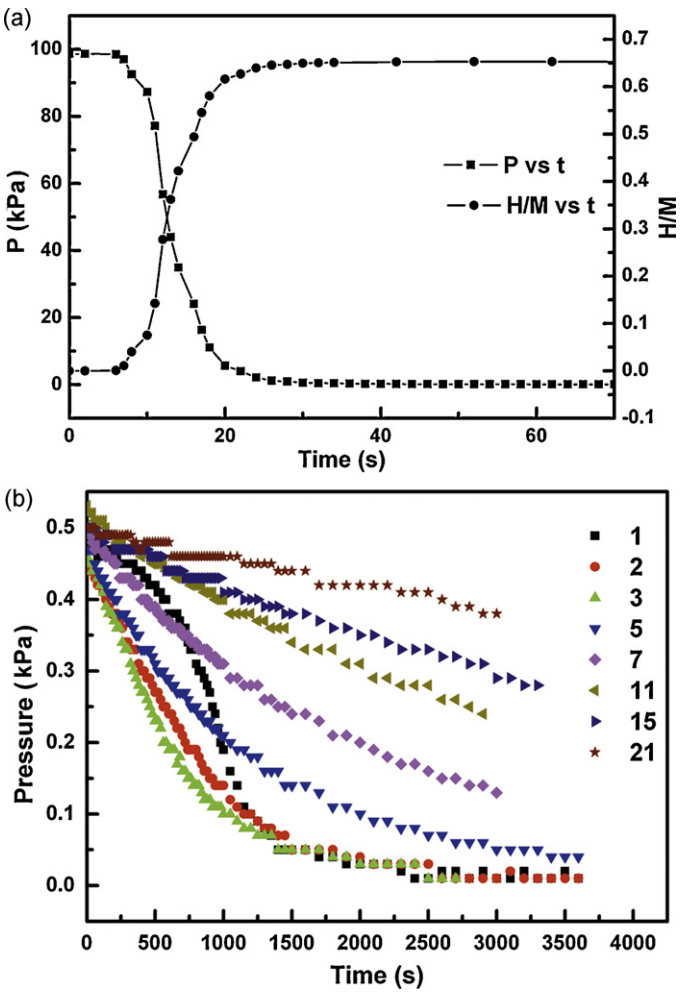

Fig. 5. (a) Initial activation curves of ScCrMn alloy at P = 98.6 kPa; (b) the 21 repeated hydrogen charges for ScCrMn at the activation pressures of around 0.46 kPa.

lattice of the alloys. However, the plateau pressure of ScCrMn is much lower than that of ZrMnCr. The difference in chemical affinity to hydrogen is likely to be the dominant factor, and the perfect close-packed structure of ScCrMn may also play a role in this case.

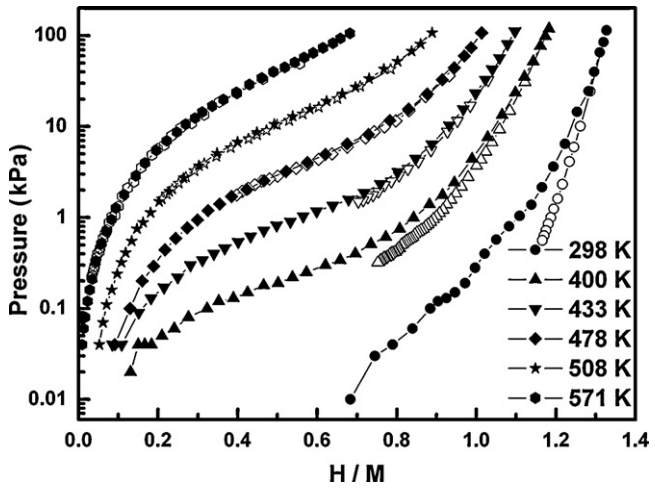

Fig. 6. P–C isotherms for ScCrMn alloy at different temperatures. The solid symbols are for the absorption curves, whereas the corresponding open symbols are for the associated desorption curves.

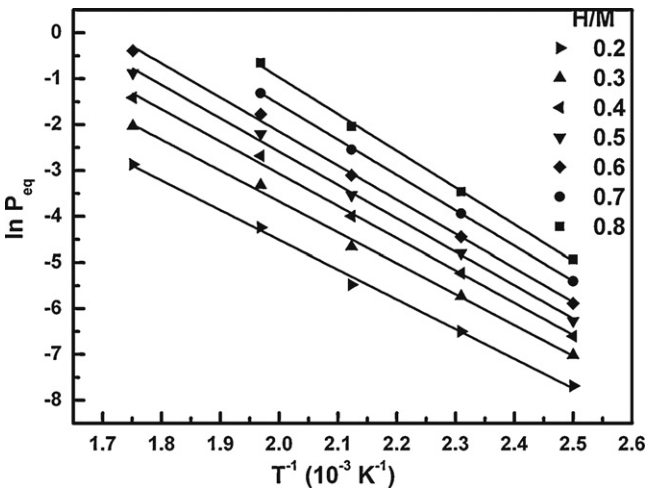

Fig. 7. Van't Hoff plots of ScCrMnH$_x$ at 298–571 K.

3.2.3. Thermodynamic characteristics

The relative partial molar enthalpy ΔH and entropy ΔS of hydride formation for ScCrMn alloy are derived from least-squares fits and extrapolations of the Van't Hoff plots of ln P_{eq} vs. $1/T$ in the $\alpha + \beta$ two-phase region as a function of hydrogen concentration. The fits are displayed in Fig. 7, and the calculated ΔH and ΔS for different H/M ratios are listed in Table 3, where equilibrium pressure P_{eq} at room temperature is derived by setting up T at 298 K. It is obvious that the absolute values of ΔH and ΔS increase with the increasing hydrogen concentration indicated by H/M. The practical significance of ΔH value is to evaluate the thermo-chemical stability of the hydride. For ScCrMn–H_2, the ΔH with H/M = 0.66 at plateau pressure is -63.0 ± 1 kJ/mol, which is relatively large and indicates a stable hydride. Quantitatively, the derived ΔH values are comparable to those of ZrCo (-54.6 kJ/mol at H/M = 0.5) [25] and $ZrTi_{0.2}V_{1.8}$ (-60 kJ/mol at H/M = 0.65) [26]. The ZrCo, $ZrTi_{0.2}V_{1.8}$ and similar alloys with large hydrogen absorption capacity and high stability have been preferable for isotope storage and purification applications. However, the activations of these alloys require high temperature and/or high pressure. In addition to the comparable hydrogen absorption properties, the ScCrMn alloy exhibits extremely easily activation properties. Therefore, the alloy would be superior to these alloys for the relevant applications.

3.2.4. DSC–TG analysis

The DSC and TG measurements shown in Fig. 8 provide some additional information on the release of hydrogen and other gases captured in the hydride of the alloy. The observed endothermic peak P_1 and the corresponding weight loss of 2.33 wt% indicate the occurrence of a phase transformation during the hydrogen releasing process, consistent with transformation of the high hydrogen concentration β hydride into the low hydrogen concentration α hydride and the pristine alloy. In comparison, the total hydrogen concentration in the hydride sample derived from the RH-404

Table 3
The thermodynamic parameters and equilibrium pressure at room temperature.

H/M	ΔH (kJ/mol H_2)	ΔS (J/mol H_2 K)	P_{eq} (10^{-1} Pa)
0.2	−53.7	−70.0	1.73
0.3	−55.9	−81.2	2.81
0.4	−58.3	−91.1	3.45
0.5	−60.4	−99.3	3.98
0.6	−61.7	−106	4.99
0.66	−63.0	−111	5.36
0.7	−64.0	−115	6.20
0.8	−66.5	−125	7.43

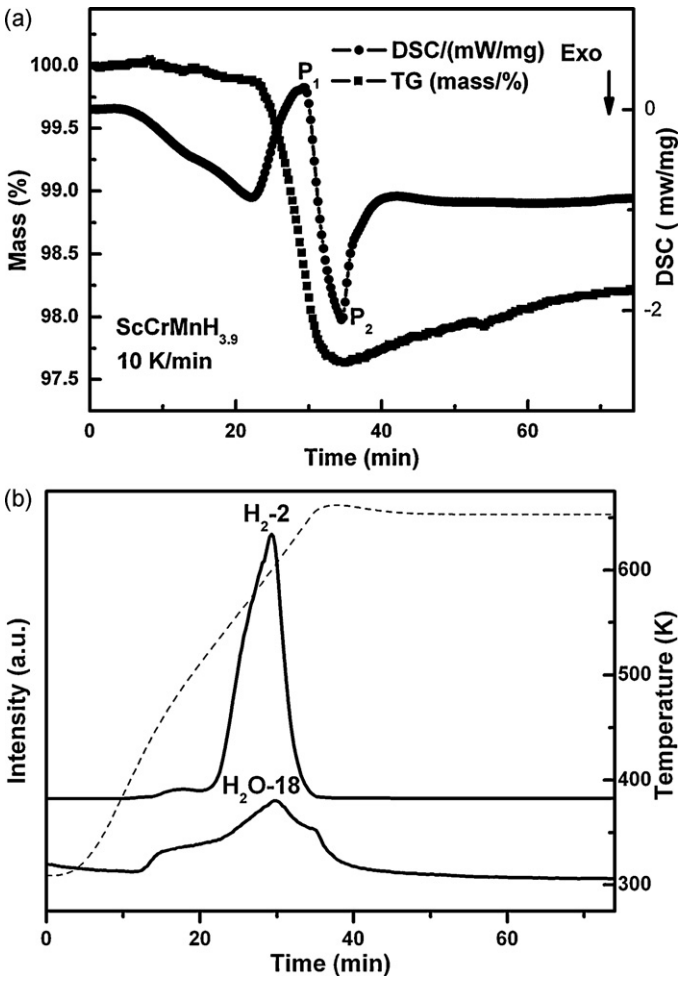

Fig. 8. DSC–TG results for a ScCrMn alloy specimen hydrogenated at 100 kPa after three cycles of hydrogen absorption/desorption, (a) DSC and TG vs. time curves, (b) mass spectrum (full) and heating (dash) vs. time curves. In the mass spectrum of H_2O-18, the intensity is scaled for 5 times, and qualitatively reliable.

hydrogen determinator is 2.5 wt%, corresponding to a hydride of $ScMnCrH_{3.9}$. Since the hydride sample measured by the determinator is under atmospheric condition consistent with that of the XRD sample, the hydrogen concentration value of $ScMnCrH_{3.9}$ has been used for the above XRD measurement. The small difference of 0.17 wt% between the DSC–TG and determinator measurements may be attributed to the residual hydrogen retained in the hydride sample after DSC–TG measurements. However, considering the measurement deviations and possible counterbalance weight gain due to minor oxidation of the dehydrogenated sample surface in DSC–TG measurement, it is estimated that the total hydrogen in the hydride can basically be released at 653 K. As shown in Fig. 8(b), the detected mass spectrums suggest that only hydrogen and H_2O vapor are released during the heating of hydride. Since the P_1 peak is attributed to the release of hydrogen, the following P_2 peak is likely to have some association with the formation of the H_2O vapor. The H_2O vapor can come from the release of the adsorbed H_2O on the hydride and/or the combination reaction of the released hydrogen and residual oxygen in the system. Since the release of adsorbed H_2O from a hydride is not an exothermic process, the exothermic feature of the negative peak P_2 at higher temperatures can only be attributed to an oxidation reaction, in which the residual oxygen in the system could oxidize either the ScCrMn to form relevant metal oxides or the released hydrogen to form H_2O. The formation of metal oxides will result in a mass gain on the TG curve, whereas there is no such effect for the formation of H_2O. However, the nonoccurrence of a corresponding mass peak, but the presence of a continuous mass gain of about 0.5 wt% in the TG curve at the holding temperatures of 653 K indicates that the formation of metal oxides is not the cause of the exothermic peak P_2. Moreover, the initial release of H_2O at temperature well above boiling point and the extension of the final release of H_2O to the high temperature far beyond that of hydrogen also support the formation of H_2O vapor by oxidation of released hydrogen. The extremely easy hydrogen activation property demonstrated by the alloy has indicated that the alloy is an effective catalyst for hydrogen dissociation. The observation of the reaction of hydrogen with residual oxygen in the system to form H_2O vapor in the presence of the alloy at moderate temperatures of 420–653 K suggests that the alloy is also effective for the catalysis of oxidation reaction.

4. Conclusions

(1) ScCrMn alloy crystallizes in C14 type Laves phase structure, with $a = 5.064(1)$ Å and $c = 8.263(2)$ Å. The structure parameters of the alloy indicate a rarely ideal close-packed Laves phase structure, though the ANOE of the alloy deviates from the ANOE dependent rule on Laves phase structure. The hydride of the alloy $ScCrMnH_{3.9}$ has a unit cell 27% larger than the alloy, but keeps the same close-packed structure. The hydride possesses a high degree of crystallinity with minimal defects, and the hydrogen appears to be homogeneously distributed in the evenly distributed interstitials of the hydride.

(2) ScCrMn alloy is endowed with extremely easy activation properties. The alloy can be activated at a low pressure of 0.46 kPa and exhibit very fast absorption rate at sub-atmosphere at room temperature, indicating that the alloy is an effective catalyst for the dissociation of hydrogen.

(3) Hydride of ScCrMn alloy exhibits very low hydrogen equilibrium pressure. The stability of the hydride is comparable to those of the hydrogen isotope storage alloys of ZrCo and $ZrTi_{0.2}V_{1.8}$. The alloy is superior to those alloys on relevant applications due to its better activation properties.

(4) The total release of hydrogen in the hydride of ScCrMn alloy can basically be achieved at 653 K, the released hydrogen can react with oxygen to form water on the surface of the alloy at moderate temperatures, implying that the alloy is also effective for catalysis of oxidation.

Acknowledgements

The authors are grateful to Mingqiang Tang for sample fabrication, Jingjing Li for TEM examination and Xufeng Gao for DSC–TG measurements. A helpful discussion with Professor Xiuliang Ma on electron diffraction patterns is also appreciated.

References

[1] J.H. Kim, H. Lee, K.T. Hwang, J.S. Han, Int. J. Hydrogen Energy 34 (2009) 9424.
[2] S.V. Mitrokhin, J. Alloys Compd. 404–406 (2005) 384.
[3] A. Pebler, E.A. Gulbransen, Trans. Metall. Soc. AIME 239 (1967) 1593.
[4] J.G. Park, H.Y. Jang, S.C. Han, P.S. Lee, J.Y. Lee, J. Alloys Compd. 325 (2001) 293.
[5] X.M. Guo, E.D. Wu, J. Alloys Compd. 455 (2008) 191.
[6] X.M. Guo, E.D. Wu, Rare Metals 25 (2006) 218.
[7] M.X. Gao, H. Miao, Y. Zhao, Y.F. Liu, H.G. Pan, J. Alloys Compd. 484 (2009) 249.
[8] Y. Moriwaki, T. Gamo, T. Iwaki, J. Less-Common Met. 172 (1991) 1028.
[9] A.L. Shilov, M.E. Kost, N.T. Kuznetsov, J. Less-Common Met. 105 (1985) 221.
[10] M. Yoshida, E. Akiba, J. Alloys Compd. 226 (1995) 75.
[11] M. Yoshida, H. Ishibashi, K. Susa, T. Ogura, E. Akiba, J. Alloys Compd. 230 (1995) 100.
[12] M. Yoshida, H. Ishibashi, K. Susa, T. Ogura, E. Akiba, J. Alloys Compd. 226 (1995) 161.
[13] T. Zotov, E. Movlaev, S. Mitrokhin, V. Verbetsky, J. Alloys Compd. 459 (2008) 220.

[14] B.A. Hunter, C.J. Howard, LHPM: A Computer Program for Rietveld Analysis of X-ray and Neutron Powder Diffraction Patterns, ANSTO Report, 1998.
[15] E. Tal-Gutelmacher, N. Eliaz, D. Eliezer, D. Zander, L. Jastrow, U. Köster, Mater. Sci. Eng. A 358 (2003) 219.
[16] R.P. Elliott, W. Rostoker, Trans. Am. Soc. Met. 50 (1958) 617.
[17] http://chemistry.about.com/library/blperiodictable.htm (currently available).
[18] E.H. Kisi, C.E. Buckley, E.M. Gray, J. Alloys Compd. 185 (1992) 369.
[19] V. Iosub, J.-M. Joubert, M. Latroche, R. Cerný, A. Percheron-Guégan, J. Solid State Chem. 178 (2005) 1799.
[20] U.I. Chung, J.Y. Lee, Acta Metall. Mater. 38 (1990) 811.
[21] E. Wicke, J. Blaurock, J. Less-Common Met. 130 (1987) 351.
[22] M.H.H. Van, Ph.D. Dissertation, Technische Hogeschool Delft, Netherlands, 1976.
[23] A. Jain, R.K. Jain, G. Agarwal, I.P. Jain, J. Alloys Compd. 438 (2007) 106.
[24] X.M. Guo, Ph.D. Thesis, Chinese Academy of Sciences, 2008 (in Chinese).
[25] N. Bekris, U. Besserer, M. Sirch, R.-D. Penzhorn, Fusion Eng. Des. 49–50 (2000) 781.
[26] X.W. Yang, T.B. Zhang, R. Hu, J.S. Li, X.Y. Xue, H.Z. Fu, Int. J. Hydrogen Energy 35 (2010) 11981.